Adiabatic self-heating determination for Ti6Al4V at different temperatures

A. Sela[a,*], G. Ortiz-de-Zarate[a], D. Soler[a], G. Germain[b], L. Gallegos[b], P.J. Arrazola[a]

[a] *Faculty of Engineering, Mondragon Unibertsitatea, 20500 Arrasate, Spain*
[b] *Arts et Métiers Campus d'Angers, LAMPA EA1427, 2 bd du Ronceray, 49000 Angers, France*

Abstract

Nowadays, predictive models are one of the most widely used techniques to predict material performance subjected to different manufacturing processes. However, to carry out accurate predictions, these models require reliable input data which are obtained from thermomechanical tests. Nevertheless, the majority of the work employed during plastic deformation is transformed into heat. This heat is dissipated to the surroundings and just a small amount is stored in the deformed sample, making the temperature of the sample to change during the test. In this context, the adiabatic heating, that could be defined as the ratio between the heat spent to heat the sample to the plastic work is a key parameter. This parameter is commonly taken as 0.9 and it is usually used by commercial finite element software. However, many authors took a different approach, defining the adiabatic heating as the ratio between the heat experimentally measured to the total plastic work. This second approach is neglecting heat losses and could lead to an underestimation of this coefficient. In addition, both approaches are used indistinctly which could lead to misunderstandings. Thus, the aim of this paper is to measure the adiabatic heating coefficient for Ti6Al4V sample being deformed using a Gleeble thermomechanical simulator. A 3D thermodynamic analysis was carried out, taking into account heat losses by different sources such as radiation, convection, conduction or mass fluxes.

Keywords: Adiabatic self-heating, Infrared measurement, thermodynamic analysis, Ti6Al4V, compression test

1. Introduction

Material characterization of metal alloys is commonly carried out through thermomechanical tests. For example, by using Gleeble thermomechanical simulator, which enable high heating rates and accurate thermomechanical loading,

*Corresponding author:
Email address: asela@mondragon.edu (A. Sela)

the heating being controlled through Joule effect [1]. However, in practice, it is quite impossible to reach pure isothermal conditions due to heat conduction along the sample, conduction between anvils and sample and possible losses into the surroundings (convection and conduction) [2].

Bennet et al. [3] demonstrated that the stress measurements could differ more than 20% due to inhomogeneous temperature along the sample. This could lead to misprediction on the material properties as stated by Evans and Scharning [4]. This thermal gradient could also have influence on sample microstructure [5]. Therefore, during thermomechanical characterization, a proper temperature control is essential. When the strain rate is low, usually lower than $0.001\ s^{-1}$, the process could be assumed as isothermal as there is enough time to dissipate the heat. Contrary, at higher strain rates, higher than $10\ s^{-1}$, the process can be assumed nearly adiabatic. In the intermediate regime, the process is neither adiabatic nor isothermal [6, 7].

Temperature is usually measured through thermocouples. For instance, Xiao et al. [2] carried out a comprehensive study to show the relevance of thermal gradients during material characterization. However, the thermal gradient was measured based on two thermocouples distributed along the sample, which could not reflect the thermal field properly. Similarly, Kardoulaki et al. [8] or Semiatin et al. [9] studied the effect of thermal gradients because of resistance heating by welding three thermocouples along the sample. Shao et al. [10] determined the heat flux along the sample during tensile testing with six thermocouples evenly distributed. This approach notably hampers the data treatment but could be more realistic on representing the thermal gradient. Thermocouples, however, influence the heat flow acting as thermodynamic fins, they have limited transient response and they only allow single point measurements to be done [11, 12]. In addition, the spatial resolution of thermocouples is notably limited, making them an unsuitable option when high thermal gradients are expected [13].

To address these issues, higher spatial resolutions could be obtained through infrared cameras, which can be used to measure thermal fields. In comparison with thermocouples, this technique presents many advantages such as being a non-intrusive technique with a very fast response. However, the main disadvantage lies in the fact that sources of error such as emissivity, reflections, absorption and obstructions need to be controlled [14]. Van Rooyen et al. [13] showed that for high-strain-temperature process this technique is more useful than thermocouples to control process temperature.

Together with a proper thermal control of the test, it is worth mentioning that during plastic deformation the part being deformed is self-heated because of this high deformation. The majority of the work employed in the deformation is transformed into heat (phenomenon known as adiabatic self-heating) whereas a small amount is kept as stored energy in lattice and contributes to the development of dislocation structures [7, 15]. This temperature rise directly influences the performance of the thermomechanical test as it affects the flow curve of the material [16]. In addition, it may not only affect the mechanical properties of the material but also the material microstructure, as stated by [17]. Therefore,

the control and knowledge of this temperature rise is a key aspect on the performance of the thermomechanical characterization and to develop any accurate FEM model.

Within this context, different definitions could be found in literature representing this phenomenon which, in this work, have been distinguished as β_1 and β_2. The adiabatic self-heating, β_1, could be defined as it was early done by Taylor and Quinney [18], as the ratio between the heat spent to heat the sample to the plastic work done. This definition has been used for years and it is usually taken as 0.9-0.95 [19, 7, 20]. This range of values is widely accepted and many commercially available FEM software such as Deform, AdvantEdge or Forge NXT uses it. For instance, Mathieu et al. [21] or Cuesta et al. [22] included this coefficient in their thermal analysis. Nevertheless, other researchers defined the adiabatic self-heating as the ratio between the heat experimentally observed via thermal variations to the total plastic work done [23, 24, 25], β_2 in this research. Under pure adiabatic conditions, these definitions would lead to the same result, however, when heat losses play an important role (at low strain rates or at high temperatures) the values reported by each definition could differ notably.

Although both definitions of adiabatic self-heating are acceptable, it is necessary to establish a proper way to characterize it. In literature, both definitions are used indistinctly, which could lead to misunderstandings. See on Table 1 the variation reported in literature for Ti6Al4V.

Table 1: Different values of adiabatic self-heating found in literature for Ti6Al4V under different conditions. Tests carried out at room temperature

Load mode	Strain rate (s^{-1})	Def.	β	Reference
Shear	460	β_2	0.2-0.7	[26]
Compression	3000	β_2	0.5-1.0	[27]
Compression	3000	β_2	0.4	[28]
Compression	2000	β_2	0.4-0.5	[24]
Tension	1500-3400	β_2	0.3-0.4	[24]
Shear	2800-7000	β_2	0.4-0.5	[24]
Tension	500-7000	β_2	0.5-0.6	[29]
Tension	0.001-0.01	β_1	0.6-0.9	[7]
Compression	1-50	β_1	0.9-0.98	[30]

Several attempts were found in literature aiming to measure adiabatic self-heating. According to an early study from Zhao et al. [31], the temperature variation during a compression test is a result from the combination between the heat generated by plastic deformation, the heat produced due to friction and the heat loss through conduction between the sample and the dies. This approach was tested at 300°C over a wide range of strain rates. In the study, heat losses due to radiation and convection were assumed to be negligible, which, even at 300°C, could be a risky assumption leading to a bad estimation of the adiabatic self-heating coefficient.

Rittel et al. [24] characterized the adiabatic self-heating for different materials, strain rates and load modes at room temperature. In spite of the comprehensive study carried out, heat losses such as conduction were not included in the analysis, which could explain the low values of adiabatic self-heating obtained at these elevated strain rates. The adiabatic self-heating was directly determined according to the temperature measurements, that is, β_2.

Bonk et al. [20] performed tensile tests in a vacuum chamber to avoid convection losses. The temperature was measured through different K-thermocouples distributed along the region of interest. Similar approach was taken by Knysh and Korkolis [7] avoiding the necessity of controlling what was happening outside the region of interest. The temperature was measured with an infrared camera whereas Digital Image Correlation was used to determine possible heat losses due to mass flux. However, both approaches were carried out at low strain rates, typical from tensile tests but far different from industrial conditions.

Also, the temperature is a relevant aspect to be taken into consideration when characterizing this coefficient [32, 33] as higher temperatures imply higher heat losses. Therefore, a proper way to characterize it at high temperatures would be needed as it is briefly analysed in literature. Likewise, [24] demonstrated the dependence of this parameter on the loading mode and the material, also proving that even at strain rates higher than 1000 s^{-1}, β_2, could be far different from 1.

Thus, although adiabatic self-heating was experimentally measured by different researchers, no agreement was found between them. In addition, the majority of the tests were made at low temperatures (up to 300°C to the best of our knowledge) although it was demonstrated that it can notably vary with temperature due to the increase on heat losses. Regarding the techniques employed on the adiabatic self-heating characterization, thermal imaging or thermocouple measurements are the most widely used. However, as it was explained above, thermocouples embedded to the specimen may change the heat flux and they only allow single point measurements to be done. Thus, infrared imaging seems to be the best option. In addition, heat losses play an important role so they should be included in the analysis.

This paper aims to show a technique to measure the adiabatic heating for an aeronautical alloy (Ti6Al4V), considering heat losses by radiation, convention and conduction. The technique proposed considers a 3D control volume containing the region of interest (the region of shear strain localization) according to DIC measurements. High speed infrared filming allows the evolution of the process to be determined and the adiabatic heating was obtained at different stages of the compression tests. The effect of temperature was also analysed within the paper.

The paper is organized as follows. The first section shows the the physical background, employed methods and used approximations to compute the adiabatic self-heating coefficient (heat losses, approaches). Then, the description of the experimental set-up is presented. Following, the results are presented and discussed and, finally, the conclusions are shown.

2. Theoretical basis

To carry out material characterization, the material is plastically deformed by controlling some physical parameters such as temperature, compression load and displacement, which define plastic strain and strain rate.

However as stated above, due the to the energy conservation law, the sample temperature may change during the test. If a control volume is considered, during the test, the sample is subjected to a mechanical work, i.e. a certain amount of energy is introduced into the system that has to be either dissipated or stored into this volume. The amount of energy introduced by the deformation process, W_p, can be calculated by equation (1)

$$W_p = \int_0^{L_f} F dL \tag{1}$$

where F is the compression load and L is the displacement, that is, the area under the force curve obtained from the Gleeble tests.

According to the schematic view of the energy balance shown in figure 1, this energy is transformed as given by equation 2.

$$W_p = Q_m + Q_{cond} + Q_{conv} + Q_{rad} + Q_{mt} + E_{stored} \tag{2}$$

where each term of this equation (2) is explained and analysed in the following paragraphs.

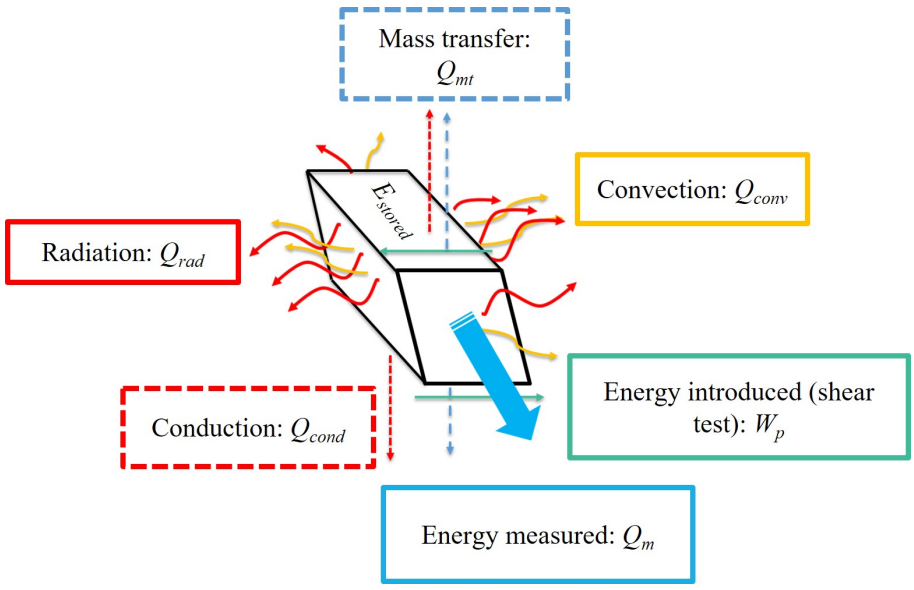

Figure 1: Control volume considered for the adiabatic self-heating calculus

Q_m is the heat associated with the temperature rise measured with the infrared camera in the 3D control volume and can be determined according to equation (3).

$$Q_m = \rho c_p V \Delta T_{IR} \tag{3}$$

where ρ and c_p are the density and the specific heat capacity of the material, assumed to be constant during the test, V is the volume of the shear zone (control volume) and ΔT_{IR} is the temperature rise measured with the infrared camera.

Q_{cond} is referred to the heat transfer between the control volume and the rest of the sample by conduction (see Figure 1). This heat loss can be quantified by equation (4).

$$Q_{cond} = \rho c_p V d_\alpha \frac{\partial^2 T}{\partial x_i^2} = kV \frac{\partial^2 T}{\partial x_i^2} \tag{4}$$

where d_α is the thermal diffusivity of the material, T is the temperature, x_i represents the coordinate referred to the heat flux direction and k is the heat conduction. $\dfrac{\partial^2 T}{\partial x_i^2}$ was determined based on infrared measurements.

Q_{conv} and Q_{rad} are the heat losses of the volume control into the surroundings, representing the convection energy and the losses due to radiation, respectively. Convection losses can be calculated by equation (5).

$$Q_{conv} = A_{loss} h (T_{surf} - T_{air}) \tag{5}$$

where A_{loss} is the section of losses, this means the section in direct contact with the air, h is the heat convection coefficient of the air, which was set to 10 $\mathrm{W/m^2K}$ according to [34], T_{surf} is the average temperature of the sample measured with the infrared camera and T_{air} is the temperature of the surroundings (room temperature), both measured in K.

Likewise, the energy loss due to radiation is given by equation (6).

$$Q_{rad} = A_{loss} \varepsilon_{em} \sigma_{SB} (T_{surf}^4 - T_{air}^4) \tag{6}$$

where ε_{em} is the emissivity of the surface and σ_{SB} is the Stefan-Boltzmann's constant.

Q_{mt} is related to the mass exchange between the control volume and the surroundings. However, with the help of a high speed filming camera and an image correlation software it was shown that this heat loss was negligible in the present work.

Finally, E_{stored} is referred to other aspects such as restoration processes (dynamic recrystallization, recovery), the development of dislocation structures or stored lattice energy.

Therefore, the adiabatic self-heating can be expressed by equation (7) [7].

$$\beta_1 = \frac{Q}{W_p} \tag{7}$$

which can be calculated as:

$$\beta_1 = \frac{Q_m + (Q_{cond} + Q_{conv} + Q_{rad} + Q_{mt})}{W_p} \tag{8}$$

Alternatively, several authors, defined the adiabatic self-heating as the ratio between the heat measured via the temperature variation and the plastic work, i.e.

$$\beta_2 = \frac{Q_m}{W_p} \tag{9}$$

3. Experimental set-up

Uniaxial compression loading of the specimens was carried out using a Gleeble 3500 thermo-mechanical testing machine. The specimens were located between two tungsten carbide anvils. The friction between the anvils and the specimen was negligible thanks to the use of graphite sheets. The vacuum chamber was opened so the process could be filmed. Therefore, vacuum was not created. This leads to heat losses due to convection and could cause the oxidation of the samples. Although oxidation could change the emissivity of the surface, this was constantly controlled through thermocouple measurement and IR camera comparison.

The machine heats the specimen based on the Joule effect with a heating rate of 10°C/s up to the desired temperature. The testing temperature was held constant for 30 s to ensure the homogeneity along the sample. The temperature was controlled through a K-thermocouple welded to the specimen (see Figure 2). In the present case, these temperatures were room temperature (RT) and 600°C. The Gleeble machine records the force through a Kistler dynamometer and the displacement during the process, in order to analytically determine the plastic strain.

The specimen employed consisted of a shear sample similar to the one shown in [1]. The compressed distance was 2 mm and the speed was kept constant and set to 1.9 mm/s to keep the strain rate constant during the experimental test.

All the tests were filmed with a frame rate of 9000 frames per second using a Photron FASTCAM APX-RS250K. The objective used was a Navitar 12X. The sample was lit with HMI HSL 250 cool light (see Figure 2a). Thanks to high speed filming, it was proven that the volume of the shear zone remained almost constant during the test, variations being lower than 5%.

To carry out Digital Image Correlation (DIC) measurements from this surface, a speckle pattern was created. Different painting methods were tested to ensure good adhesion under the tested conditions, with enough resolution and no decorrelation problems. The aim of these measurements was to properly determine the shear zone and to obtain the strain fields. DIC analysis was done using GOM Correlate software. The noise error on plastic stain measurements was quantified by analysing the equivalent plastic strain obtained between 100 frames without movement.

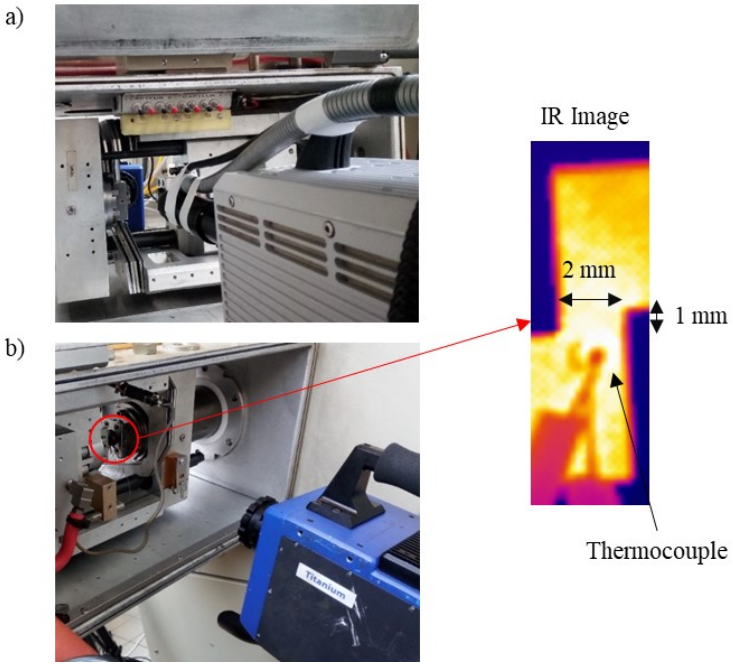

Figure 2: Experimental set-up: a) Photron FASTCAM APX-RS250K with HMI HSL 250 cool light; b) FLIR Titanium 550M with focus on the shear zone (infrared image) and the K-thermocouple

Infrared images of the sample being deformed were taken using the FLIR Titanium 550M with 1000 Hz of sampling frequency. The emissivity was characterized thanks to the thermocouple welded to the surface as Figure 2b shows. At high temperatures, the effect of reflected temperature was totally negligible and the emissivity could be directly determined by comparing infrared and thermocouple measurements. However, at room temperature the effect of reflected temperature must be properly characterized. In this case, the diffuser reflector method was employed [35]. The self-heating of the material was used as the heating source and the anvil reflection was employed to estimate the reflected temperature (see Figure 3). For this specific case, the reflected temperature was 32°C.

Finally, material microstructure was analysed so as to study the existence of some changes in the microstructure due to the deformation process. The deformed samples were mounted on resin and polished up to mirror finishing. Then, they were etched with Kroll's reagent to reveal the microstructure. For each sample geometry, the undeformed microstructure was compared with the deformed one at each temperature.

The material employed was the alloy Ti6Al4V, provided as a hot rolled bar with a diameter of 80 mm. The material was delivered in the annealed condition. Figure 4 shows the microstructure with primary α grains and $\alpha + \beta$

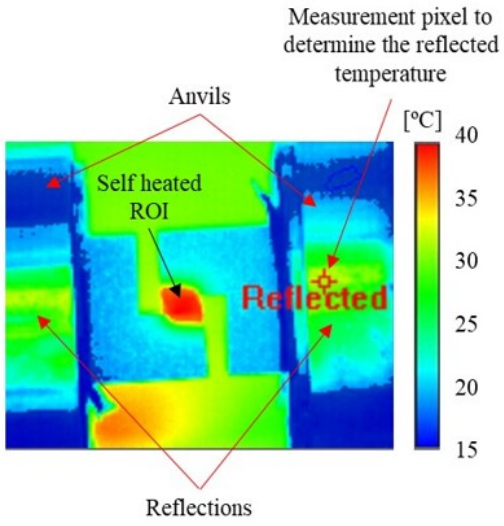

Figure 3: Determination of the reflected temperature. Apparent temperatures given in Celsius degrees (ROI: Region of Interest)

colonies with an average grain size of 10.5 ASTM. The measured microhardness was $350HV_{0.05}$. The density was 4430 kg/m^3 and the chemical composition is summarized in Table 2.

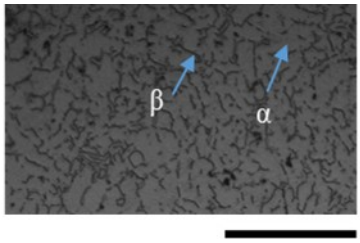

Figure 4: Initial microstructure of the Ti6Al4V employed. Scale bar: 50 µm

Material properties were taken from literature [36, 37, 38], being the specific heat capacity 519 and 680 J/kgK and the heat conductivity 6.7 and 10 W/mK, at room temperature and at 600°C, respectively.

4. Results and discussion

4.1. Force analysis

The force results for each condition are shown in Figure 5. The area within the curve represents the plastic work done (after removing the elastic effect). Two totally different behaviours were observed at the two temperatures. When

Table 2: Chemical composition of the Ti6Al4V

Element	V	Al	Fe	C	O	N	Ti
Weight percent	4.05	6.36	0.16	0.015	0.019	0.006	Bal.

the test was carried out at room temperature, the flow behaviour shows the typical strain hardening behaviour up to drastic brittle failure when the displacement is close to 1 mm.

In contrast, higher ductility was observed at 600°C and no macroscopic failure seemed to take place. In addition, there is a decrease in the force when the displacement is close to 0.5 mm, which can be related to restoration microstructural processes such as dynamic recrystallization due to deformation at high temperature.

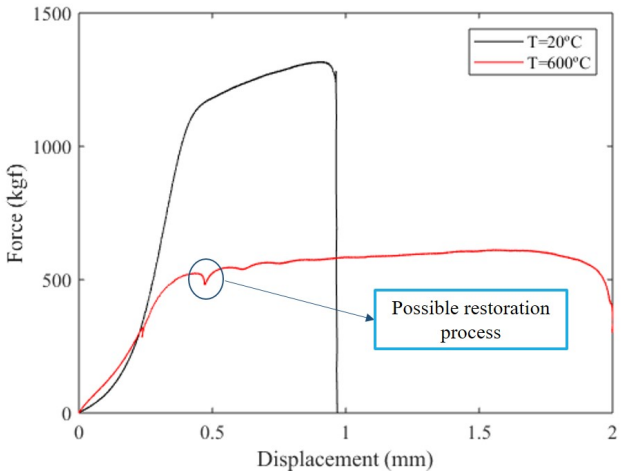

Figure 5: Force-displacement diagrams

4.2. Digital image correlation analysis

The main aim of carrying out DIC analysis is to determine the volume of the shear zone in order to define the control volume and the area of losses so as to be applied in equations (1)-(6). The relevance of the losses due to mass transfer will be also analysed considering the speed component on Y direction.

The method employed to create the pattern was speckle painting technique as it is widely accepted because of its simplicity and cheapness. The test at 600°C was taken as reference to test the different possibilities. The aim was to find a proper technique to obtain a surface with a good speckle pattern in order to measure strain at high temperatures. Therefore, the goal was to check the capability of the technique of being employed (in terms of adhesion, brightness or paint crack) rather than create the best possible speckle pattern.

Eight different techniques were tested varying the surface finishing between polishing (etched and not), wire electro discharge machining (WEDM) surface and sandblasting. White speckles were randomly sprayed with Molydal NB 25 which consists of small particles of boron nitride. This paint works at temperatures up to 1000°C. Some of the surfaces were previously painted black trying two different paintings, PYRO FEU matt black anti-caloric paint, resistant at high temperatures (up to 900°C) and AREMCO HiE-Coat 840-MX ceramic-based which is a black pigmented coating for metals up to 1300°C.

Among all the techniques tested, at high temperature, the best technique found consisted of: (i) the WEDM surface was directly painted in black with AREMCO HiE-Coat 840-MX; (ii) the painting was cured to ensure good adhesion; (iii) white speckles were randomly spread along the surface with Molydal NB 25. For the tests at room temperature, the procedure was similar but the AREMCO black paint was substituted by PYRO-FEU 24950-6 900°C thermal paint, making the curing process unnecessary at this temperature.

Measurements were carried out using GOM Correlate software. After determining the best option to create the speckle pattern, the quality was analysed using software criterion as it is shown in Figure 6. The noise error on plastic stain measurements was quantified the variation of plastic strain between these 100 frames being lower than 0.005 for the whole set of conditions tested.

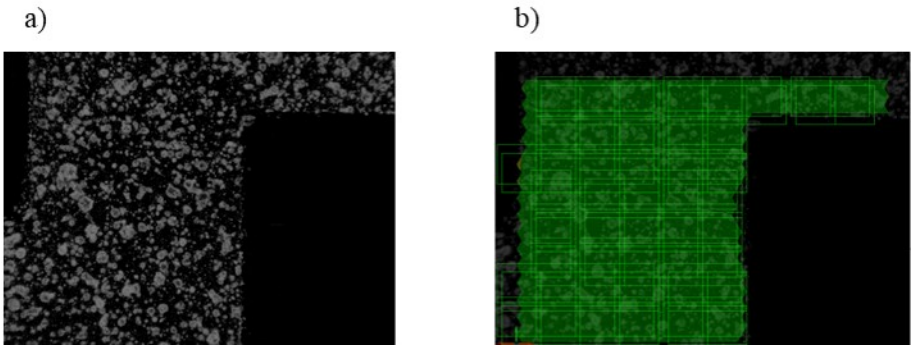

Figure 6: a) Example of an speckle pattern employed for DIC analysis (at 600°C). b) Quality of the speckle pattern created according to GOM Correlate software

The speckle sizes were in the range from 0.02 to 0.12 mm. Because of the intense distortion expected (due to severe shear strain), the subset size was set to 60 pixels (which is 0.35 mm) with a step size of 20 pixels according to [39]. The subset size is the width of the square to mesh the reference image. The step size is the distance between subset centres.

As an example, a picture of the DIC measurements is shown in Figure 7, the strain field obtained is similar to the ones shown in [40, 41] so the shear approach is assumed to be valid for the study. As can be seen, the shear zone can be approximated by a parallelepiped and its dimensions lead to a volume of 21 mm^3.

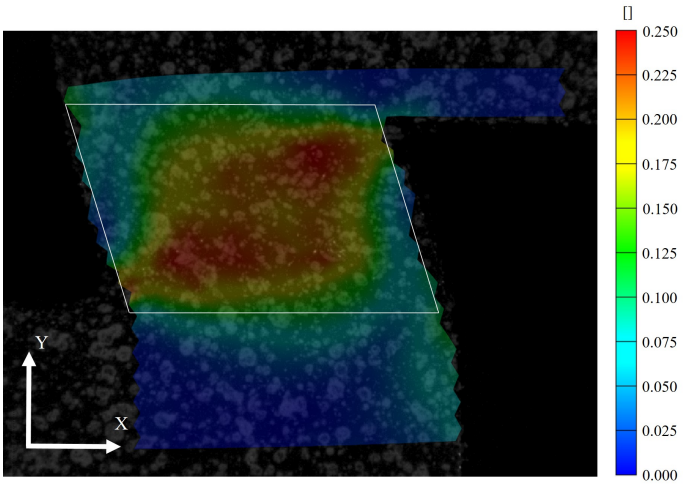

Figure 7: Equivalent plastic strain field (T=600°C)

It is worth mentioning that the volume was observed to remain almost constant during deformation, once the shear zone has been formed, at both temperatures. The measured thickness of the shear zone, based on the equivalent strain field, was 1.38 mm.

The possible material fluxes into and out of the control volume may influence heat losses and could be relevant in the calculus of the adiabatic self-heating. Therefore, it is necessary to determine whether some particles tend to travel out of the control volume. To carry out this estimation, the possible existence of velocity in Y direction would be a proper indicator. It is worth noting that compression forces are applied in horizontal direction according to the coordinates shown in Figure 7. The velocity field in Y direction is shown in Figure 8. At 600°C no presence of velocity in Y direction was found. The same result was obtained at 20°C. Thus, the heat losses due to mass transfer (Q_{mt}) can be neglected.

4.3. Surface temperature analysis

The temperature evolution of a point located in the centre of the shear zone was determined by tracking a 3x3 pixel. Figure 9 shows the increment of the temperature with respect to the programmed one, that is, RT and 600°. It can be observed that the measured temperature increment is slightly higher in the room temperature case whereas the heating rate is notably higher.

To calculate heat losses due to convection (Q_{conv}) and radiation (Q_{rad}) the average temperature of the whole shear zone for each taken thermogram was used. For instance, in Figure 10 it can be seen the temperature evolution taking different measurement protocols, with no remarkable variation between the single point and the ROI measurement. However, it could be also observed

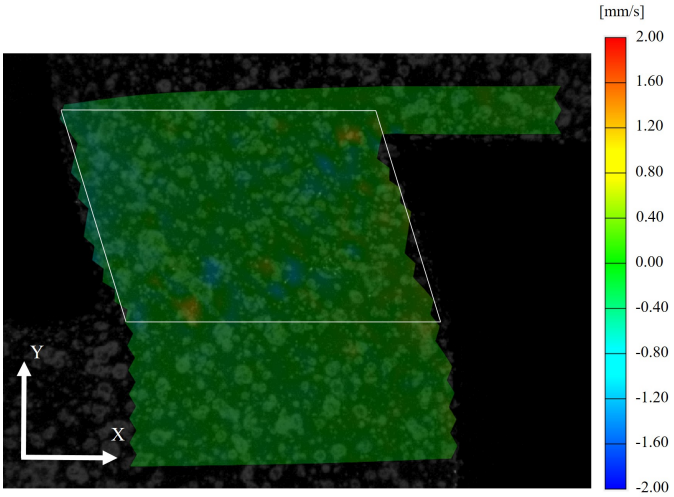

Figure 8: Velocity in vertical direction: v_y field (T=600°C)

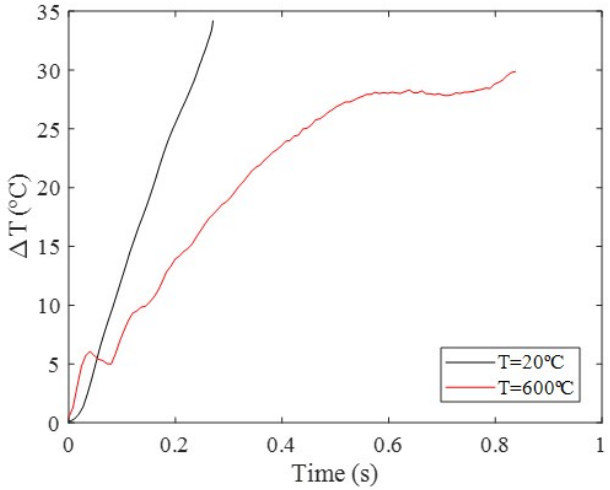

Figure 9: Temperature rise during the process in the centre of the shear zone

how the use of thermocouples could give wrong values, as the measurement strongly depends on the position of the thermocouple among other issues.

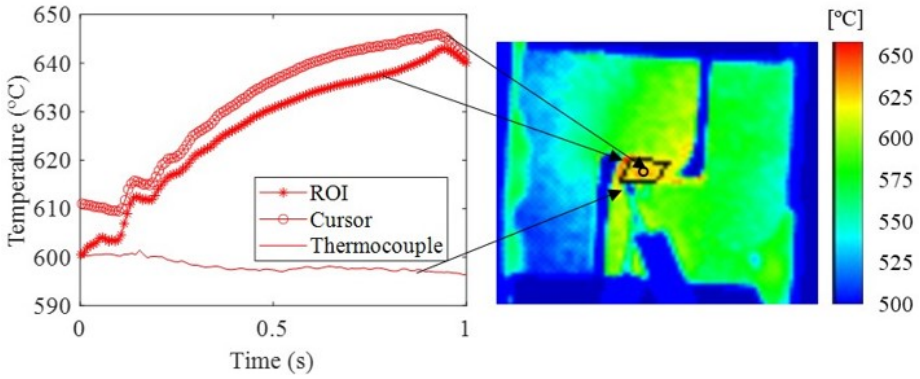

Figure 10: Temperature evolution during a thermomechanical test (sample tested at 600°C). $u_T = \pm$ 30°C

In order to also estimate the heat losses due to conduction it is necessary to determine $\frac{\partial^2 T}{\partial x_i^2}$. Based on infrared measurements, the conduction flux along the shear zone can be reduced to a flux in Y direction as Figure 11 shows.

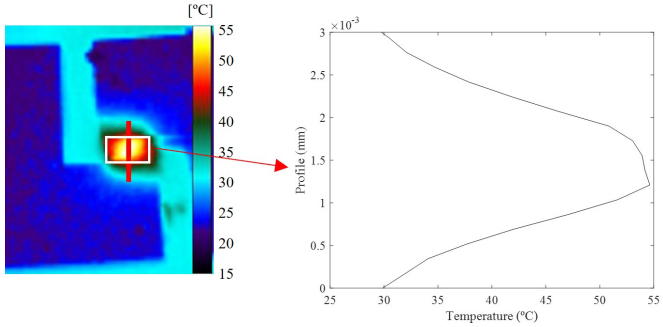

Figure 11: Left: Temperature field within the shear zone at 20°C. Right: Temperature profile along Y direction to determine heat losses due to conduction

Based on Figure 11 (right side), it can be seen how the temperature profile along the shear zone is symmetric. Therefore, in order to numerically calculate $\frac{\partial^2 T}{\partial x_i^2}$ (being $x_i = Y$ in the present case) the shear zone was divided into two halves. The average value of $\frac{d^2 T}{dY^2}$ was numerically calculated for each half at each frame. Finally, heat conduction losses can be estimated by transforming Equation 4 into Equation 10.

$$Q_{cond} = 2(k\frac{V}{2}\frac{d^2T}{dY^2}) \tag{10}$$

4.4. Determination of adiabatic self-heating

The results obtained at 20°C are shown in Figure 12. First of all, it is worth highlighting that radiation and convection losses were observed to be negligible under these conditions as they always represented less than 0.1 % of the whole energy. The term named as "others" represent the residual in which E_{stored} is included.

The average value of β_1 during the whole test was 0.88 which is in agreement with the values reported in literature [7]. In this case, the conduction losses progressively increase with time, reaching close to 5% of the total energy introduced. The value of β_2, calculated only considering Q_m and W_p was close to 0.84. With respect to the term "others", its value is around 10%, which could be related to the stored energy in terms of microstructural aspects.

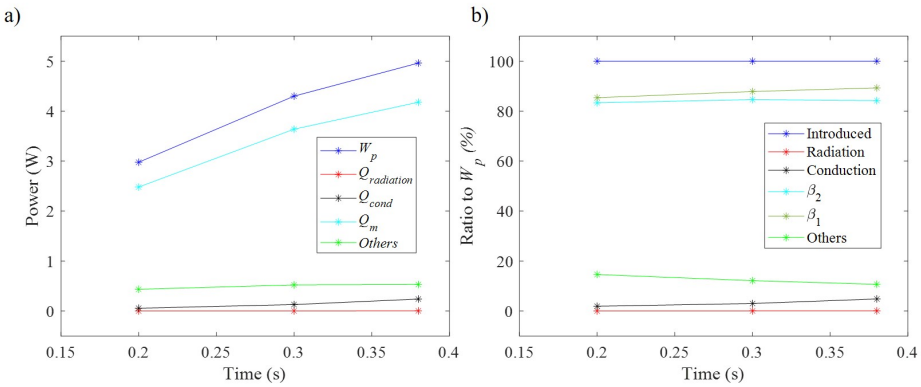

Figure 12: Room temperature: a) Calculus of power including all possible heat losses, b) heat losses as a percentage of W_p

According to different authors, Ti6Al4V suffers flow instabilities and inhomogeneous flow at room temperature which may lead to adiabatic shear bands, resulting in local melting and fracture [42, 43]. In Figure 13 the initial and final microstructure at room temperature can be compared. It can be seen, in the final microstructure, a thin affected layer in which the microstructure is oriented in the fracture direction (probably an adiabatic shear band) which could explain the stored energy.

The same analysis was carried out at 600°C as Figure 14 shows. Under this condition, radiation represents more than 20% of all of the heat losses so this term has to be considered in the analysis to calculate the adiabatic self-heating coefficient. Convection losses could be also relevant, representing around the 5% of the heat losses as a first approach.

The average value of β_1 was 0.87, again in agreement with the values reported in literature [7]. However, the value of β_2 was 0.57 due to the high level

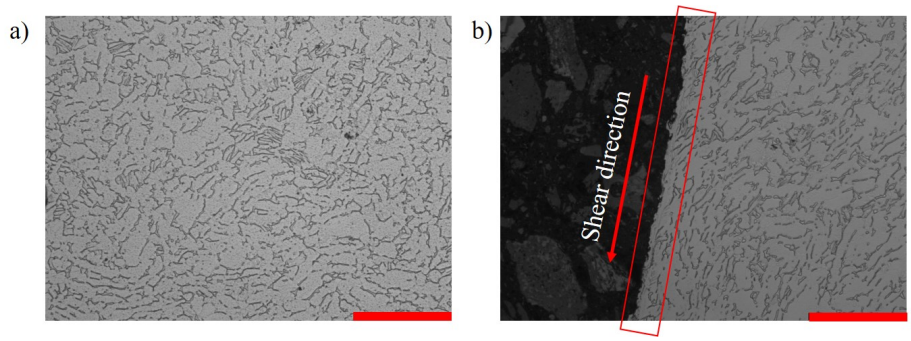

Figure 13: Room temperature: a) Initial microstructure of Ti-6Al-4V (α+β structure), b) Microstructure after fracture: affected zone. Scale bar: 50 μm. Magnification: 500X

of losses. Therefore, it can be seen how, when the heat losses are not relatively relevant (in the room temperature case radiation and convection losses are totally negligible), the values of β_1 and β_2 are quite close. These conditions are typical for tests carried out at high strain rates or at low temperatures. Finally, it was observed that the term "others", again, represents around the 10% of all energy. As in previous case, under these conditions, adiabatic shear banding is expected [44].

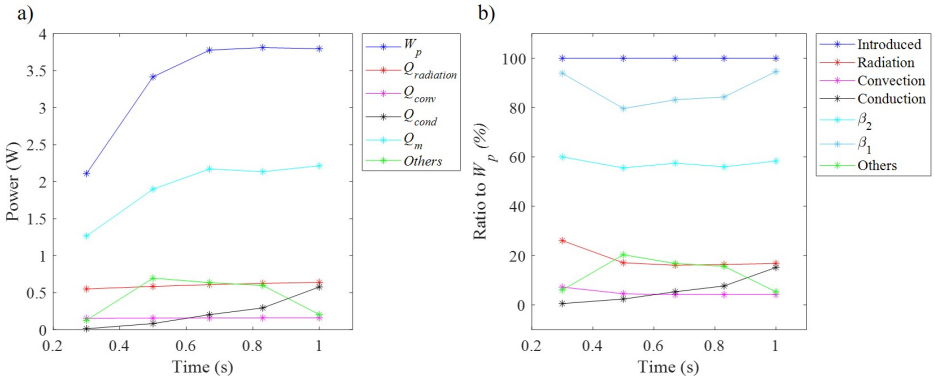

Figure 14: T = 600°C: a) Calculus of power including all possible heat losses, b) heat losses as a percentage of W_p

The microstructure before and after the deformation test is shown in Figure 15. As it can be seen, the initial microstructure did not present any remarkable different compared with the one shown in Figure 13a, so the heating up to 600°C does not imply any phase change in the material, just causing an increase in the grain size. In contrast, as the ductility was observed to be higher (see Figure 5) no drastic failure was observed. Although the crack has started, it has not enough time to propagate and cause the drastic failure. Again, the microstructure shows the orientation in the direction of the shear force, which

could explain the amount of energy stored. In addition, grain elongation could be observed close to the shear banding zone, which could be an indicator of dynamic recovery, as some authors reported [45, 46].

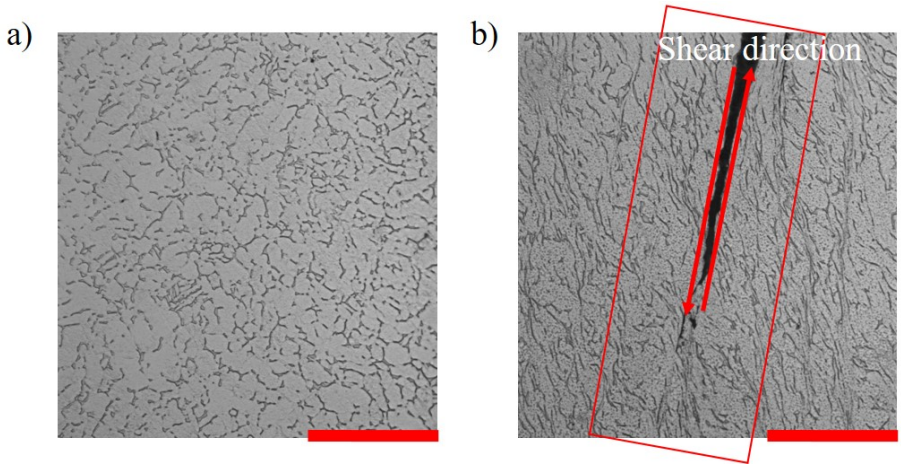

Figure 15: T = 600°C: a) Initial microstructure of Ti-6Al-4V (α+β structure), b) Microstructure after deformation: affected zone. Scale bar: 50 μm. Magnification: 500X

The amount of energy stored was proved to be constant in the range of temperatures from 20 to 600°C, the adiabatic heating coefficient (β_1) being close to the widely reported 90% under both conditions. As this parameter is important in numerical simulations, if the model is able to take into account thermal losses such as radiation or convection, its value can be assumed to be 0.9 whereas if the model does not include this, something typical for 2D models, its value should be corrected as radiation losses could represent more than 20% of all energy introduced in the system. In addition, this parameter is also relevant in material characterization as it determines the real temperature at which the test was carried out.

5. Conclusions

After analysing all the results, the following conclusions can be drawn:

- A technique to measure the adiabatic self-heating under shear conditions with a 3D control volume is proposed considering heat losses and the energy measured through infrared measurement at different temperatures, demonstrating its capability at low and high temperatures.
- The adiabatic heating, β_1, was demonstrated to be close to 0.9 as it is widely reported in literature under both conditions. This parameter is relevant on numerical simulations and can be set to 0.9 if the model is able to take into account heat losses such as convection or radiation.

- Different approaches were found in literature defining the adiabatic heating value. With this methodology, it was shown that, although β_1 remains almost constant at different temperatures, the value of β_2, due to the relevance of the heat losses, is notably lower when the temperature increases.

Acknowledgements

The authors would like to thank the project SURFNANOCUT (RTI2018-095463-B-C21 and RTI2018-095463-B-C22) and the grant for Education and Training of Research Staf (FPU 17/02498).

References

[1] A. Hor, F. Morel, J.-L. Lebrun, G. Germain, An experimental investigation of the behaviour of steels over large temperature and strain rate ranges, International Journal of Mechanical Sciences 67 (2013) 108–122.

[2] H. Xiao, X. Fan, M. Zhan, B. Liu, Z. Zhang, Flow stress correction for hot compression of titanium alloys considering temperature gradient induced heterogeneous deformation, Journal of Materials Processing Technology 288 (2021) 116868.

[3] C. Bennett, S. Leen, E. Williams, P. Shipway, T. Hyde, A critical analysis of plastic flow behaviour in axisymmetric isothermal and gleeble compression testing, Computational materials science 50 (1) (2010) 125–137.

[4] R. Evans, P. Scharning, Axisymmetric compression test and hot working properties of alloys, Materials science and technology 17 (8) (2001) 995–1004.

[5] G.-Z. Quan, J. Pan, Z.-h. Zhang, Phase transformation and recrystallization kinetics in space–time domain during isothermal compressions for ti–6al–4v analyzed by multi-field and multi-scale coupling fem, Materials & Design 94 (2016) 523–535.

[6] M. Mataya, V. Sackschewsky, Effect of internal heating during hot compression on the stress-strain behavior of alloy 304l, Metallurgical and Materials Transactions A 25 (12) (1994) 2737.

[7] P. Knysh, Y. P. Korkolis, Determination of the fraction of plastic work converted into heat in metals, Mechanics of materials 86 (2015) 71–80.

[8] E. Kardoulaki, J. Lin, D. Balint, D. Farrugia, Investigation of the effects of thermal gradients present in gleeble high-temperature tensile tests on the strain state for free cutting steel, The Journal of Strain Analysis for Engineering Design 49 (7) (2014) 521–532.

[9] S. Semiatin, D. Mahaffey, N. Levkulich, O. Senkov, The radial temperature gradient in the gleeble® hot-torsion test and its effect on the interpretation of plastic-flow behavior, Metallurgical and Materials Transactions A 48 (11) (2017) 5357–5367.

[10] Z. Shao, N. Li, J. Lin, T. A. Dean, Strain measurement and error analysis in thermo-mechanical tensile tests of sheet metals for hot stamping applications, Proceedings of the Institution of Mechanical Engineers, Part C: Journal of Mechanical Engineering Science 232 (11) (2018) 1994–2008.

[11] A. Hoyne, C. Nath, S. Kapoor, Cutting temperature measurement during titanium machining with an atomization–based cutting fluid (acf) spray system, in: ASME 2013 International Mechanical Engineering Congress and Exposition, American Society of Mechanical Engineers, 2013, pp. 1–10.

[12] H.-J. Kröning, U. Lang, N. Hofmann, High temperature gleeble microtensile testing of metallic micro specimens, Materials Testing 58 (10) (2016) 826–832.

[13] M. van Rooyen, T. H. Becker, High-temperature tensile property measurements using digital image correlation over a non-uniform temperature field, The Journal of Strain Analysis for Engineering Design 53 (3) (2018) 117–129.

[14] D. Soler, P. Aristimuño, A. Garay, P. J. Arrazola, Uncertainty of temperature measurements in dry orthogonal cutting of titanium alloys, Infrared Physics & Technology 71 (2015) 208–216.

[15] A. Zubelewicz, Century-long taylor-quinney interpretation of plasticity-induced heating reexamined, Scientific Reports 9 (1) (2019) 1–7.

[16] A. Chrysochoos, O. Maisonneuve, G. Martin, H. Caumon, J. Chezeaux, Plastic and dissipated work and stored energy, Nuclear Engineering and Design 114 (3) (1989) 323–333.

[17] F. Feng, S. Huang, Z. Meng, J. Hu, Y. Lei, M. Zhou, D. Wu, Z. Yang, Experimental study on tensile property of az31b magnesium alloy at different high strain rates and temperatures, Materials & Design 57 (2014) 10–20.

[18] G. I. Taylor, H. Quinney, The latent energy remaining in a metal after cold working, Proceedings of the Royal Society of London. Series A, Containing Papers of a Mathematical and Physical Character 143 (849) (1934) 307–326.

[19] S. Dumoulin, H. Louche, O. Hopperstad, T. Børvik, Heat sources, energy storage and dissipation in high-strength steels: Experiments and modelling, European Journal of Mechanics-A/Solids 29 (3) (2010) 461–474.

[20] C. Bonk, M. Vucetic, A. Bouguecha, B. A. Behrens, An experimental-numerical method to determine the plastic work converted into heat applied on ahss, in: Advanced Materials Research, Vol. 1140, Trans Tech Publ, 2016, pp. 51–58.

[21] G. Mathieu, V. Frederic, R. Vincent, F. Eric, 3d stationary simulation of a turning operation with an eulerian approach, Applied Thermal Engineering 76 (2015) 134–146.

[22] M. Cuesta, P. Aristimuño, A. Garay, P. Arrazola, Heat transferred to the workpiece based on temperature measurements by ir technique in dry and lubricated drilling of inconel 718, Applied Thermal Engineering 104 (2016) 309–318.

[23] Z. Pan, B. Sun, V. P. Shim, B. Gu, Transient heat generation and thermo-mechanical response of epoxy resin under adiabatic impact compressions, International Journal of Heat and Mass Transfer 95 (2016) 874–889.

[24] D. Rittel, L. Zhang, S. Osovski, The dependence of the taylor–quinney coefficient on the dynamic loading mode, Journal of the Mechanics and Physics of Solids 107 (2017) 96–114.

[25] S. Härtel, M. Graf, B. Awiszus, K. G. Abstoss, R. Hild, Novel approach for the determination of the taylor-quinney coefficient, in: Materials Science Forum, Vol. 918, Trans Tech Publ, 2018, pp. 103–109.

[26] D. Macdougall, J. Harding, The measurement of specimen surface temperature in high-speed tension and torsion tests, International journal of impact engineering 21 (6) (1998) 473–488.

[27] J. Mason, A. Rosakis, G. Ravichandran, On the strain and strain rate dependence of the fraction of plastic work converted to heat: an experimental study using high speed infrared detectors and the kolsky bar, Mechanics of Materials 17 (2-3) (1994) 135–145.

[28] D. Rittel, Z. Wang, Thermo-mechanical aspects of adiabatic shear failure of am50 and ti6al4v alloys, in: Engineering Systems Design and Analysis, Vol. 48357, 2008, pp. 529–550.

[29] J. L. Smith, J. D. Seidt, A. Gilat, Full-field determination of the taylor-quinney coefficient in tension tests of ti-6al-4v at strain rates up to 7000 s^{-1}, in: Advancement of Optical Methods & Digital Image Correlation in Experimental Mechanics, Volume 3, Springer, 2019, pp. 133–139.

[30] S. Bruschi, S. Poggio, F. Quadrini, M. Tata, Workability of ti–6al–4v alloy at high temperatures and strain rates, Materials Letters 58 (27-28) (2004) 3622–3629.

[31] D. Zhao, Temperature correction in compression tests, Journal of materials processing technology 36 (4) (1993) 467–471.

[32] S. Oh, S. Semiatin, J. Jonas, An analysis of the isothermal hot compression test, Metallurgical transactions A 23 (3) (1992) 963–975.

[33] R. Goetz, S. Semiatin, The adiabatic correction factor for deformation heating during the uniaxial compression test, Journal of materials engineering and performance 10 (6) (2001) 710–717.

[34] A. Shitzer, Wind-chill-equivalent temperatures: regarding the impact due to the variability of the environmental convective heat transfer coefficient, International journal of biometeorology 50 (4) (2006) 224–232.

[35] R. Usamentiaga, P. Venegas, J. Guerediaga, L. Vega, J. Molleda, F. G. Bulnes, Infrared thermography for temperature measurement and non-destructive testing, Sensors 14 (7) (2014) 12305–12348.

[36] J. J. Li, W. L. Johnson, W.-K. Rhim, Thermal expansion of liquid ti–6al–4v measured by electrostatic levitation, Applied physics letters 89 (11) (2006) 111913.

[37] M. Boivineau, C. Cagran, D. Doytier, V. Eyraud, M.-H. Nadal, B. Wilthan, G. Pottlacher, Thermophysical properties of solid and liquid ti-6al-4v (ta6v) alloy, International journal of thermophysics 27 (2) (2006) 507–529.

[38] N. Milošević, I. Aleksić, Thermophysical properties of solid phase ti-6al-4v alloy over a wide temperature range, International journal of materials research 103 (6) (2012) 707–714.

[39] I. D. I. C. Society, A good practices guide for digital image correlation (2018).

[40] Y. Bao, T. Wierzbicki, On fracture locus in the equivalent strain and stress triaxiality space, International Journal of Mechanical Sciences 46 (1) (2004) 81–98.

[41] C. Leitao, M. Costa, K. Khanijomdi, D. Rodrigues, Assessing strength and local plastic behaviour of welds by shear testing, Materials & Design 51 (2013) 968–974.

[42] S. V. Kailas, Y. Prasad, S. Biswas, Flow instabilities and fracture in ti-6al-4v deformed in compression at 298 k to 673 k, Metallurgical and materials transactions a 25 (10) (1994) 2173–2179.

[43] Y.-M. Luo, J.-X. Liu, X.-W. Cheng, S.-K. Li, F.-C. Wang, W.-W. Guo, Adiabatic shear banding of hot-rolling ti–6al–4v alloy subjected to dynamic shearing and uniaxial dynamic compression, Rare Metals 34 (9) (2015) 632–637.

[44] N. Reddy, Y.-H. Lee, J. H. Kim, C. S. Lee, High temperature deformation behavior of ti- 6al- 4v alloy with and equiaxed microstructure: a neural networks analysis, Metals and materials International 14 (2) (2008) 213.

[45] S. Roy, S. Suwas, The influence of temperature and strain rate on the deformation response and microstructural evolution during hot compression of a titanium alloy ti–6al–4v–0.1 b, Journal of Alloys and Compounds 548 (2013) 110–125.

[46] L. Mosecker, A. Göttmann, A. Saeed-Akbari, W. Bleck, M. Bambach, G. Hirt, Deformation mechanisms of ti6al4v sheet material during the incremental sheet forming with laser heating, in: Key Engineering Materials, Vol. 549, Trans Tech Publ, 2013, pp. 372–380.